Proceedings of the 17th World Congress
The International Federation of Automatic Control
Seoul, Korea, July 6-11, 2008

Physical-Model-Based Control of a Piezoelectric Tube Scanner

P. J. Gawthrop * **B. Bhikkaji** ** **S. O. R. Moheimani** **,[1]

* *Centre for Systems and Control and Department of Mechanical Engineering, University of Glasgow, GLASGOW. G12 8QQ Scotland.*

** *School of Electrical Engineering and Computer Science, The University of Newcastle, Newcastle, NSW 2308, Australia.*

Abstract: A piezoelectric tube is shown to have linear, but non-minimum phase dynamics. The main impediment to the actuation of this piezoelectric tube is the presence of a low-frequency resonant mode which causes mechanical vibrations. A physical-model-based control method is extended to non-minimum phase systems in general and successfully applied to damp the resonant mode; leading to a vibration-free actuation of the piezoelectric tube.

1. INTRODUCTION

Scanning Tunneling Microscopes (STMs) and Atomic Force Microscopes (AFMs) are used extensively in diverse areas of science such as crystallography, cell biology, etc,. When used at extreme magnifications they are capable of generating topographical maps of solid surfaces at micro to atomic resolution. In many commercially available STMs and AFMs a probe is placed in close proximity, typically a few nanometers, to the material surface for which a topographical map is desired. And the given surface is scanned by moving the sample in a raster pattern, so that the probe interacts with the entire region of interest. In general, scanning is performed by placing the sample on top of a piezoelectric tube, and actuating the tube in a raster pattern.

Under certain experimental conditions the dynamics of the piezoelectric tube can be approximated by linear models, see Daniele et al. (1999). The linear models normally reveal the presence of lightly damped resonance modes, which make the piezoelectric tubes susceptible to mechanical vibrations. Non-linear phenomenon such as creep and hysteresis also become visible when actuating the tube using low frequency inputs and high amplitude inputs respectively. In such scenarios the linear approximations become inadequate. The objective of this paper is to perform fast scans using a piezoelectric tube actuator of the type typically used in scanning probe microscopes. The main impediments to fast scanning are the presence of mechanical vibrations and hysteresis.

The use of feedback control to compensate for vibrations in the piezoelectric tubes has been investigated by several authors Daniele et al. (1999). As in the case of any other flexible structure, it is desirable to have controllers that are easy to implement, robust to variations in plant parameters, and rolls-off in the high frequency regions.

Hysteresis becomes visible when piezoelectric tubes are actuated using voltage signals of high amplitudes. A popular approach to compensate for hysteresis is to model it as a non-linear function, $H(\cdot)$, and then eliminate it by cascading its inverse $H^{-1}(\cdot)$, see Venkataraman et al. (2000). Since the late 1980's, it has been known that actuating piezoelectric transducers with current or charge sources, rather than voltage sources, significantly reduces hysteresis Kaizuka et al. (1988); Fleming et al. (2006). In this paper the latter approach is taken to compensate for hysteresis and keep the linear approximation.

In the setup used here, one side of the piezoelectric tube is used for actuation, and the other for sensing. It turns out that this asymmetric actuation leads to significant complications which make feedback control a more challenging problem than it would otherwise be. This problem is solved in this paper.

The notion of "controller design in the physical domain" was introduced by Sharon et al. (1991) based in turn on earlier work on "impedance control" Hogan. (1985). As discussed by those papers such controllers are naturally described in bond graph Karnopp et al. (2000) terms. Such "Physical-model-based control" (PMBC) has been applied to the control of mechanical systems (Gawthrop , 2004) as well as to hybrid numerical experimental substructuring (Gawthrop , 2005). A good tutorial on this subject is presented in Gawthrop et al. (2007).

As indicated above, the dynamics of the piezoelectric tube are not only resonant but also non-minimum phase. Hitherto, the PMBC approach (Gawthrop , 2004) has been restricted to minimum-phase systems; the first purpose of this paper is to provide a novel way of extending PMBC to non-minimum phase systems. The second purpose of the paper is to apply and experimentally evaluate the PMBC approach within the context of the control of the piezoelectric tube. Thus, although the method is applied to a particular experimental system, it is applicable to mechatronic systems in general.

Section 2 summarises PMBC, section 3 gives a model of the tube and section 4 uses system identification to estimate the physical model parameters. Section 5 gives a PMBC design of a feedback controller and section 6 discusses experimental results. Section 7 concludes the paper.

2. PHYSICAL MODEL BASED CONTROL

There are three subsystems: (1) **Num** the *numerical* subsystem implemented as *software* within a digital computer (2) **Phy** the *physical* subsystem implemented as *hardware* in the physical world and (3) **Tra** the *transfer* system

[1] Corresponding author. **Reza.Moheimani@newcastle.edu.au**, Tel: +61 2 49216030, FAX: +61 2 49216993

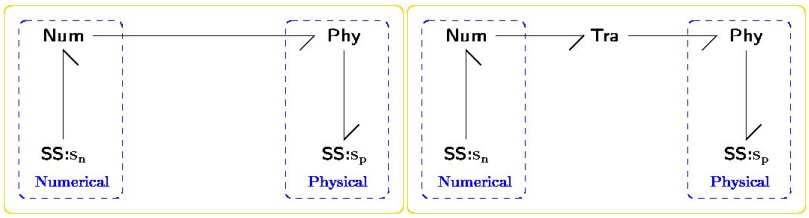

(a) (b)

Fig. 1. Physical Model Based Control. (a) The ideal collocated case. (b) The practical case where actuator and sensor dynamics are represented by the transfer system **Tra**

.

comprising sensors and actuators connecting the numerical and physical domains *together with the associated control systems and signal conditioning.*

Figure 1(a) shows the ideal case where sensors and actuators are collocated; design is relatively straightforward in this case. Unfortunately, collocation is the exception rather than the rule. Figure 1(b) shows the practical situation where either the computer imposes efforts or flows indirectly via an actuator system or the sensor is such that the measurement point and actuation point are different thus leading to non-collocation. In some cases, the problem can be removed by careful actuator design; for example, in the context of *collocated* sensor/actuator piezo patches.

In other cases, the effect of **Tra** can be removed by the design of appropriate compensation (Gawthrop , 2004). However, the particular system examined here has a right-half plane zero and it is thus non-minimum phase. As shown in Section 5, the special physical characteristics of the piezo tube system can be used to overcome the transfer system thus giving a novel approach to the PMBC of non-minimum phase systems.

Section 3 shows that the system considered in this paper can be modelled as a particular case of the structure of Figure 1.

3. MODELLING

Figure 2(a) gives a schematic diagram of the piezoelectric tube where the left-hand patch acts as an actuator and the right-hand patch as a sensor. This asymmetric actuation leads to two types of motion: a *bending mode* where a contraction of the actuation patch leads to an *extension* of the sensing patch and a vertical *piston* mode where a contraction of the actuation patch leads to a *contraction* of the sensing patch. The bending mode leads to the desired horizontal motion of the tip of the tube. The bending motion has an infinite number of vibrational modes of which only one is within the frequency range of interest; this mode can potentially lead to significant vibration problems. The piston motion is also associated with vibrational modes, but only the zero-frequency mode is within the frequency range of interest; this motion leads to the non-minimum phase behaviour.

Figure 2(b) gives the bond graph corresponding to Figure 2(a). In the frequency range of interest, the bending mode can be adequately modelled the a mass-spring-damper subsystem formed by the **I**:**m**, **C**:**k** and **R**:**r** components of Figure 2(b) whereas the piston mode has a resonance outside the frequency band of interest and can be modelled by the spring-damper system formed by the **C**:$\mathbf{k_0}$and **R**:$\mathbf{r_o}$ components of Figure 2(b).

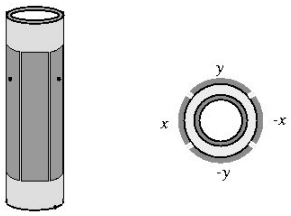

(a)

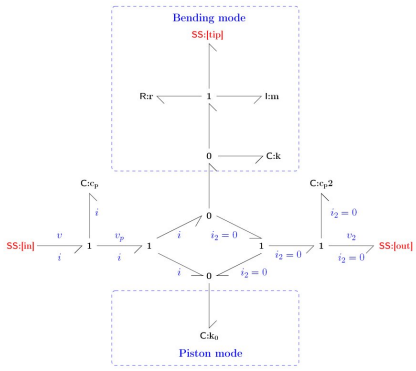

(b)

Fig. 2. Tube Modelling. v and i are the voltage and current associated with the actuation patch and v_2 and i_2 the corresponding values for the sensing patch; the components **C**:$\mathbf{c_p}$ represent the (identical) capacitances of the two patches. The mass-spring-damper components of the bending mode are **I**:**m**, **C**:**k** and **R**:**r** respectively; the piston mode is represented by **C**:$\mathbf{k_0}$and **R**:$\mathbf{r_o}$.

It is known from Fleming et al (2006) that it is advantageous to drive piezoelectric transducers with current or charge rather than voltage; furthermore, the voltage v_2 can be measured with a high-impedance instrument. Taken together, this avoids non-linear and hysteresis effects as shown in Fleming et al (2006), and the bond graph of Figure 2 represents a linear system. Energy-based modelling in general Wellstead (1979), and bond graph modelling in particular, use voltage and current (or the analogous force and velocity) as covariables. In this case, the actuator is a *charge* amplifier, and in mechanical systems the actuation is often a displacement (Gawthrop , 2005). Following an analogous approach to Gawthrop (2005), this paper develops the method as if the actuator were a current amplifier, and the resulting controller converted to charge actuation at the end of the design process.

With this form of actuation and measurement, the model of Figure 2(b) can be simplified for the purposes of control as follows. (i) The component **C**:$\mathbf{c_p}$, representing the electrical capacitance of the actuating patch can be removed as it does not effect the current i and the voltage v is not used. (ii) The component **C**:$\mathbf{c_{p2}}$, representing the electrical capacitance of the sensing patch can be removed as the current $i_2 = 0$ is zero due to the high sensor impedance. (iii) As $i_2 = 0$, the evolution of the bending and piston mode components is determined entirely by i and v_2 is a system output. These three facts mean that, as far as i, v_2 and the variables acting at the tip are concerned, the bond graph of Figure 2 can be replaced by the bond graph of Figure 3(a). As i and v_2 now appear on the same bond, these are referred to as *quasi-collocated* variables and the bond graph of Figure 3(a) as a *quasi-collocated* bond graph.

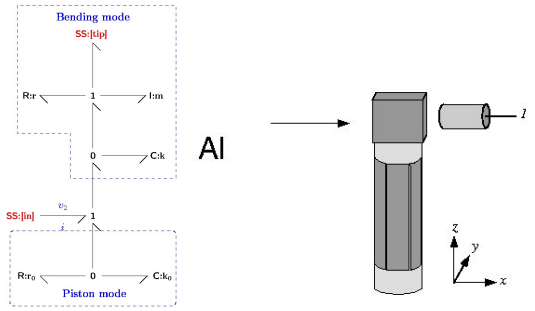

(a) (b)

Fig. 3. (a) Quasi-collocated Model. The bending mode leads to unwanted vibration and the piston mode to non-minimum phase behaviour. (b) The experimental setup with Al denoting the Aluminum cube.

The corresponding system is, however, not passive, due to the bond directed away from the piston-mode component $\mathbf{C}$:$\mathbf{k_0}$ corresponding to a spring with *negative* stiffness – it is this component that leads to the non-minimum phase nature of the system.

As discussed in section 5, this system therefore cannot be treated as **Phy** in Figure 1 of Section 2. In fact the system representing the bending mode is used as **Phy** with corresponding transfer function $P(s)$, which is the impedance of the bending mode, where:

$$P(s) = k\frac{s + \frac{r}{m}}{s^2 + \frac{r}{m}s + \frac{k}{m}}. \tag{1}$$

The transfer function relating i and v_2 can be derived from the bond graph of either Figure 2 or 3(a) as:

$$\frac{v_2}{i} = G_{vi} = \frac{k_0}{s + \alpha} - P(s) \tag{2}$$

$\alpha = \frac{k_0}{r_0}$. As mentioned previously, the system is driven by *charge*, not current Defining the *charge* associated with i as $q = \int i dt$, it follows that

$$\begin{aligned}\frac{v_2}{q} &= G_{vq} = sG_{vi} \\ &= (k_0 - k) + k\frac{\frac{k}{m}}{s^2 + \frac{r}{m}s + \frac{k}{m}} - \frac{\alpha}{s + \alpha}\end{aligned} \tag{3}$$

The first term of (3) is significant at all frequencies, the second is significant around resonance and the third term is significant at low frequencies.

4. IDENTIFICATION

4.1 Experimental setup

A jig is constructed to hold the piezoelectric tube along the z axis. A small aluminum cube is bonded to the upper end of the tube. This cube represents the seat where the materials that need to be scanned are placed. The head of an ADE Technologies 4810 capacitive sensor is placed in close proximity to the face of aluminum cube along the x axis, see Figure 3(b). The inner electrode of the piezoelectric tube is grounded. One electrode from the $x - x$ pair, referred as the x^+ electrode, is chosen as the input end of the piezoelectric tube, and the corresponding opposite end, referred as the x^- electrode, is chosen as the output end. The whole setup consisting of the piezoelectric tube with the bonded aluminum cube and the heads of the capacitive sensors, is placed in a specially constructed cylindrical enclosure. The cylindrical enclosure protects the experimental setup from external noise.

4.2 Modeling

Here, experiments are performed on the piezoelectric tube to obtain the frequency response function (FRF) $G_{vq}(\mathrm{i}\omega)$ in the frequency region $10\text{Hz} \leq f \leq 2500\text{Hz}, \omega = 2\pi f$. A parametric model of the form

$$G_{vq}(s) = \frac{\hat{K}}{s^2 + \hat{a}_1 s + \hat{a}_2} - \hat{d} \tag{4}$$

is also fitted to the experimentally determined $G_{vq}(\mathrm{i}\omega)$. The parametric form has been obtained by dropping the third term in (3) and appropriately defining the other parameters.

Using the charge amplifier swept sine waves are applied as input at the x^+ electrode of the piezoelectric tube, Figure 2(a). Application of the input swept sine causes the tube to bend, inducing a voltage signal v_2 at the x^- electrode. The input q, applied to the x^+ electrode and the corresponding output v_2 induced at the x^- are fed into a Spectrum Analyzer, which computes the frequency response function (FRF) $G_{vq}(\mathrm{i}\omega) = \frac{v_2(\mathrm{i}\omega)}{q(\mathrm{i}\omega)}$. A model of the form (4) is fit to the computed FRF. The parameters of the model are tabulated in Table 1.

Name	Value
$\hat{K}$	$2.3768. \times 10^6$
$\hat{a}_1$	46.211
$\hat{a}_2$	2.9157×10^7
$\hat{d}$	0.029854

Table 1. Empirical Transfer Function parameters

Assuming for the moment that the final term of (3) is small in the frequency band of interest, the four remaining parameters (k, k_0, m and r) of the physical model (3) can be sequentially computed from the four parameters of the empirical model (4) as $k = \frac{\hat{K}}{\hat{a}_2}, k_0 = k - \hat{d}, m = \frac{k}{\hat{a}_2}$ and $r = m\hat{a}_1$ The resultant parameters appear in Table 2.

Name	Value
k_0	0.051666 N/m
k	0.081520 N/m
m	2.7959×10^{-9} Kg
r	1.292×10^{-7}Ns/m

Table 2. Physical parameters

Note that, as the tube bends, due to the application of the input, the capacitance between the head of the capacitive sensor and the face of the aluminum cube changes. This change in capacitance is measured by the capacitive sensor in terms of the distance between its head and face of the aluminum cube. The FRF, $G_{dq}(\mathrm{i}\omega)$, relating the input $q(\mathrm{i}\omega)$ and the capacitive sensor displacement measurement $d(\mathrm{i}\omega)$ is plotted in Figure 4.

As mentioned earlier, the goal is to actuate the piezoelectric tube in a raster pattern. Therefore a desired trajectory for the piezoelectric tube would be to repeatedly trace straight lines back and forth in x direction, while slowly increasing its position in the y direction. A common practice to achieve such a path is to apply a triangular waveform to x^+ electrode and a "very slowly" increasing ramp to the

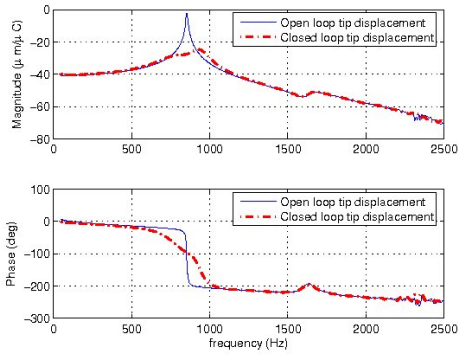

1.0

Fig. 4. Measured open and closed loop frequency responses ($G_{dq}(\mathrm{i}\omega)$ and $G_{dq}^{(cl)}(\mathrm{i}\omega)$).

y^+ electrode as reference signals for the system. Normally for illustration purposes the slowly varying ramp in the y^+ electrode is either replaced by a DC signal or assumed to be earthed or open circuited, see Daniele et al. (1999).

In Figure 5, the capacitive sensor response to a triangular waveform input with an amplitude of $5.5\mu C$ and fundamental frequency 40Hz applied at the x^+ electrode, with the y^+ electrode earthed, is plotted. The capacitive sensor output is not exactly triangular waveform, but appears to be a triangular waveform plus certain periodic corrugations. The distortion in the capacitive sensor output is due to the amplification of harmonics of the triangular waveform that are close to the resonance frequency of the piezoelectric tube.

In general to eliminate the periodic corrugations, two different approaches are taken. In the first approach, instead of using a triangular waveform, inputs to x^+ are shaped such that the output of the capacitive sensor is a triangular waveform. More specifically the input at x^+ is set to

$$u(t) \triangleq \sum_{k=1}^{N} \frac{a_k}{\mid G_{dq}(\mathrm{i}\omega_k) \mid} \sin(\omega_k t - \phi_k), \qquad (5)$$

where N is a large positive integer, $\phi_k = \angle G_{dq}(\mathrm{i}\omega_k)$, and a_k and ω_k are such that $f_d(t) = \sum_{k=1}^{\infty} a_k \sin(\omega_k t)$ is the desired triangular waveform output in the Fourier series form. The integer N is chosen such that the Fourier coefficients a_k, $k \geq N$, are numerically insignificant. It is easy to see that applying $u(t)$, (5), at x^+ would give $f_d(t)$ at the capacitive sensor output. The second approach is to use a feedback controller that would damp the resonances in $G_{vq}(s)$, and then input a triangular waveform to the closed-loop system. Note that damping the resonance peaks in $G_{vq}(s)$ would automatically suppress the amplification of the harmonics of the triangular waveform that are close to the resonance.

A first look at the two approaches would suggest that the first method is simpler than the second. However, this approach, is heavily dependent on the correctness of the model $G_{dq}(s)$, and consequently suffers from lack of robustness towards model uncertainties. In general, due to wear and tear and other external influences, piezoelectric tube characteristics such as gain and resonance frequency are prone to minor changes or perturbations. In particular, when the system's resonance frequency gets perturbed applying $u(t)$ would not result in a triangular waveform at the output. In order to incorporate a meaningful damping.

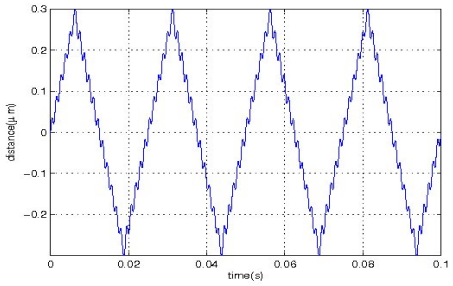

Fig. 5. Response recorded by the capacitive sensor (tip-displacement) to a triangle waveform input of amplitude $5.5\mu C$ and frequency 40Hz in open loop. The oscillations are unacceptable.

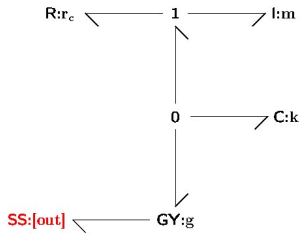

Fig. 6. Shunt controller bond graph. The **C**:**k** and **I**:**m** components are the same as in the bending mode of Figure 3(a), **R**:$\mathbf{r_c}$ dissipates the bending mode energy and **TF**:**g** provides adjustable coupling.

Here a feedback controller is constructed, linking the output x^- to the input at x^+, through the charge amplifier, to damp the vibrations. An input of the type $u(t)$, (5), is then designed for closed loop system to get the desired triangular waveform as the output.

The feedback controller is designed in the following section.

5. PHYSICAL MODEL BASED CONTROL DESIGN

With reference to Figure 1, the physical subsystem **Phy** is identified with the bending-mode portion of Figure 3(a) and the transfer system **Tra** with the piston mode and associated **1** junction. As outlined in Section 2, there are two parts to the PMBC design: designing **Num** and eliminating the effects of **Tra**. These two topics are treated in the following subsections.

5.1 Designing ***Num***

This section considers how to design the collocated controller **Num** assuming, for the moment, that k_0 is zero. There are many possibilities, but here, following Moheimani et al (2004) a resonant shunt damper is derived using a novel bond graph approach. The basic idea is to use the classical idea of attaching a mass-spring damper, tuned to the resonance frequency of a system, to extract energy from that system.

In bond graph terms, the approach of Figure 6 is natural. Comparing Figure 6 with Figure 3(a), the shunt has the same dynamic components as the bending mode model with the following changes:

(1) **R**:**r** is replaced by **R**:$\mathbf{r_c}$ where $r_c > r$ to extract energy.
(2) A **TF**:**g** component is added to dualise the shunt (as compared to the bending mode mode); this allows direct connection to the physical system without

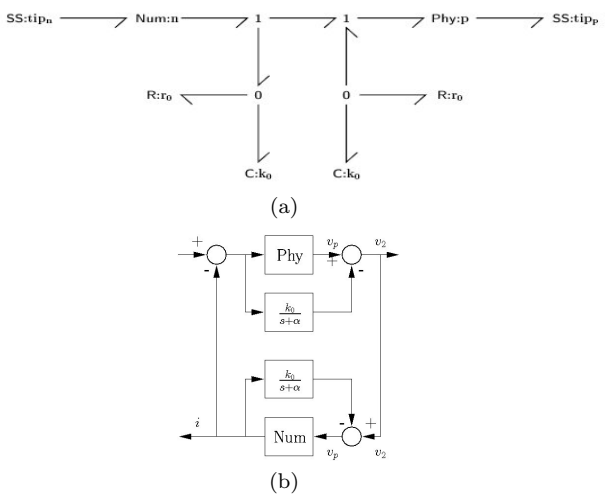

Fig. 7. Eliminating **Tra**

changing the dynamical properties. The variable gain g allows variable shunt coupling.

The corresponding transfer function is

$$N(s) = g^2 \frac{kms + r_c}{k + ms^2 + r_c s}. \tag{6}$$

This controller has two parameters (in addition to the physical parameters already specified in Table 2): the gyrator gain g and the damping r_c. As these parameters have a clear physical meaning, it was straightforward to adjust them to give a high level of damping. The chosen values are given by $g = 1.6$ and $r_c = 40r$.

5.2 Eliminating ***Tra***

As discussed in Section 3, the piston mode introduces a negative **C** and **R** component into the quasi-collocated system of Figure 3(a). The purpose of this section is, following the philosophy of Section 2, to augment the collocated controller **Num** to eliminate the effect of the unwanted negative component. Figure 7(a) gives a bond graph interpretation of the procedure suggested in this paper. **Num** is augmented with (positive) components **C**:$\mathbf{k_0}$ and **R**:$\mathbf{r_0}$ and a corresponding **1** junction. Following elementary bond graph simplification rules Karnopp et al. (2000), the two **1** junctions can be combined and the two **C**:$\mathbf{k_0}$ are then attached to the same **1** junction and can be combined to give a single **C** component corresponding to a spring of stiffness $k_0 - k_0 = 0$. The effect is then eliminated. **R**:$\mathbf{r_0}$ is eliminated similarly.

An alternative view of the same procedure is given by the block diagram of Figure 7(b) where "Num" and "Phy" now refer to the transfer functions of **Num** and **Phy** respectively. The effect of k_0 on **Num** is to add a negative *parallel* transfer function which can be removed by augmenting **Num** with a corresponding negative *feedback* transfer function. Letting $N(s)$ denote the transfer function of **Num**, it follows that the augmented controller transfer function is

$$N_a(s) = \frac{(s+\alpha)N(s)}{(s+\alpha) + k_0 N(s)} \tag{7}$$

This sort of loop transformation is to be found in a different context – stability – in, for example Desoer et al. (1975). It is known that such loop transformations are only possible if $\frac{k_0}{s+\alpha}$ is stable, ie $\alpha > 0$. For physical reasons this must be so, but the data used in Section 4 did not provide an explicit value for α, just the implied constraint that it is small in the bandwidth of the data. For this reason, α was chosen as $\alpha = 10$.

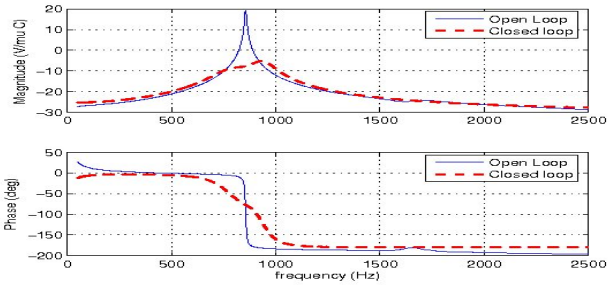

Fig. 8. Plots of $G_{vq}(\mathrm{i}\omega)$ along with $G_{vq}^{(cl)}(\mathrm{i}\omega)$, with $G_{vq}^{(cl)}(\mathrm{i}\omega)$ as in (11).

Using this value for α, together with the the physical parameters of Table 2 and the controller parameters $g = 1.6$ and $r_c = 40r$, gives the numerical value of $N_a(s)$ to be:

$$N_a(s) = \frac{0.287(s+10)(s+1848)}{s^3 + 1858s^2 + 3.025.10^7 s + 2.285.10^9} \tag{8}$$

The corresponding *charge* controller is obtained by dividing (8) by s to give:

$$\begin{aligned} N_q(s) &= \frac{0.287(s+10)(s+1848)}{s(s^3 + 1858s^2 + 3.025.10^7 s + 2.285.10^9)} \\ &\approx \frac{0.287(s+1858)}{s^3 + 1858s^2 + 3.025.10^7 s + 2.285.10^9} \end{aligned} \tag{9}$$

The latter approximation is valid around resonance and has the advantage of not containing an integrator.

Finally, the charge controller (9) is scaled by the nominal tube capacitance of $c_t = 10\mathrm{nF}$ to give the controller:

$$K(s) = \frac{2.087.10^7 s + 3.858.10^{10}}{s^3 + 1858s^2 + 3.025.10^7 s + 2.285.10^9}. \tag{10}$$

5.3 Simulation

This section looks at the properties of the controller $K(s)$ (10) in simulation.

In what follows, the effectiveness of the controller in damping the resonance in $G_{vq}(s)$ will be evaluated numerically. Experimental evaluation of the same will be done in the next subsection.

Numerical evaluation refers to comparing the open loop FRF $G_{vq}(\mathrm{i}\omega)$ with the closed loop FRF

$$G_{vq}^{(cl)}(\mathrm{i}\omega) = \frac{G_{vq}(\mathrm{i}\omega)}{1 + K(\mathrm{i}\omega)G_{vq}(\mathrm{i}\omega)}. \tag{11}$$

Here, $G_{vq}(\mathrm{i}\omega)$ and $K(\mathrm{i}\omega)$ are as in (4) and (10) respectively with $s = \mathrm{i}\omega$. Bode plots of $G_{vq}^{(cl)}(\mathrm{i}\omega)$ and $G_{vq}(\mathrm{i}\omega)$ suggests a damping of about 25dB in closed loop, refer to Figure 8. This prediction is validated experimentally in the next subsection.

6. EXPERIMENTAL RESULTS

Here, swept sine waves are applied at the x^+ electrode in closed loop with the feedback controller $K(s)$. As done

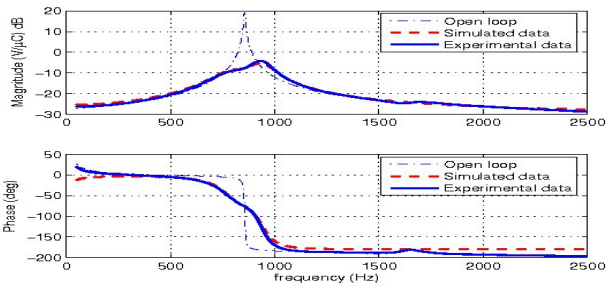

Fig. 9. The experimental closed-loop response is superimposed on the simulated open and closed-loop responses. The experimental and simulated closed loop responses are almost identical and have about 25dB more damping than the open-loop system.

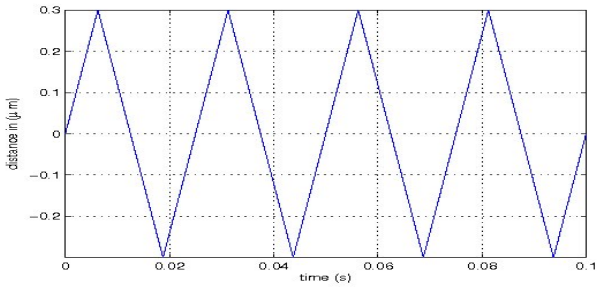

Fig. 10. Response recorded by the Capacitive sensor (tip-displacement) to a shaped input, with $f_d(t)$ being a triangular waveform of amplitude $0.3\mu m$ and fundamental frequency 40Hz. The oscillations apparent in Figure 5 have been eliminated.

in the case of the open loop in section 4, the input $q(\mathrm{i}\omega)$ and the output $v(\mathrm{i}\omega)$ are fed into the Spectrum Analyzer and the closed loop FRF $G_{vq}^{(cl)}(\mathrm{i}\omega) = \frac{v(\mathrm{i}\omega)}{q(\mathrm{i}\omega)}$ is computed. The computed closed loop is plotted Figure 9. It is apparent that experimentally determined $G_{vq}^{(cl)}(\mathrm{i}\omega)$ matches the simulated one. As the frequency response of the $G_{dq}(\mathrm{i}\omega)$, corresponding to the capacitive sensor output, and the frequency response $G_{vq}(\mathrm{i}\omega)$ share the same dynamics, one would expect the closed loop frequency response $G_{vq}^{(cl)}(\mathrm{i}\omega) = \frac{d(\mathrm{i}\omega)}{q(\mathrm{i}\omega)}$ to be also damped by the same amount. In Figure 4 the closed loop response $G_{dq}^{(cl)}(\mathrm{i}\omega)$ is plotted along with open loop response $G_{dq}(\mathrm{i}\omega)$, a 25dB damping is apparent from the plot.

Finally, to actuate the the tube in a raster pattern a shaped input of the form (5), with $G_{dq}(\mathrm{i}\omega)$ replaced by its corresponding closed loop $G_{dq}^{(cl)}(\mathrm{i}\omega)$, was applied to the x^+ electrode. As shown in Figure 10, the capacitive sensor output corresponding to this input appears to be a triangular waveform. This result is clearly an improvement on that shown in Figure 5.

7. CONCLUSION

The general approach of physical-model-based control (PMBC) has been extended to be applicable to non-minimum phase systems in general and the non-minimum phase system arising from the feedback control of a piezoelectric tube in particular.

The controller design involves the choice of only two parameters each of which has physical significance and is thus easily chosen. The resultant third-order feedback controller then follows from these two parameters as well as four physical parameters describing the piezoelectric tube. These four physical parameters can be deduced from frequency response experiments on the open-loop piezoelectric tube.

The closed-loop system frequency response predicted about 25dB of damping compared to the open-loop case. The experimentally measured frequency response matched the predicted frequency response closely. Open and closed loop experimental responses to a triangular waveform (corresponding to a fast raster scan) showed that the open-loop oscillations were largely eliminated by the closed-loop controller.

REFERENCES

A. Daniele, S. Salapaka, M. V. Salapaka and M. Dahleh. Piezoelectric Tubes for Atomic Force Microscopes: Design of Lateral Sensors, Identification and Control. *Proc. of the American Control Conference*, San Diego, California (1999) 253–257.

R. Venkataraman and P. S. Krishnaprasad Approximate Inversion of Hysteresis: Theory and Numerical Results. *Proc. of 39th IEEE Conference on Decision and Control*, (2000) 4448–4454.

H. Kaizuka and B. Siu A simple way to reduce hysteresis and creep when using piezoelectric actuators. *Japan Journal of Applied Physics*, Part 2 - Letters 27 (5) (1988) 773–776.

A. J. Fleming and S. O. R. Moheimani Sensorless Vibration Supression and Scan Compensation for Piezoelectric Tube Nanopositioners. *IEEE Transactions on Control Systems Technology*. 14 (1) (Jan 2006) 33–44.

A. Sharon, N. Hogan and D. E. Hardt Controller design in the physical domain. *Journal of the Franklin Institute*. 328 (5) (1991) 697–721.

N. Hogan Impedance control: An approach to manipulation. part I–theory. *ASME Journal of Dynamic Systems*, 107 (1985) 1–7.

D. Karnopp, D. L. Margolis, R. C. Rosenberg. System Dynamics : Modeling and Simulation of Mechatronic Systems. 3rd Edition, Horizon Publishers and Distributors Inc, 2000.

P. J. Gawthrop. Bond graph based control using virtual actuatorsy. *Proceedings of the Institution of Mechanical Engineers Pt. I: Journal of Systems and Control Engineering*218 (4) (2004) 251–268.

P. J. Gawthrop, M. Wallace, D. Wagg. Bond-graph based substructuring of dynamical systems. *Earthquake Engng Struc. Dyn.*, 34 (6) (2005) 687–703.

A. J. Fleming, S. O. R. Moheimani. Sensorless vibration suppression and scan compensation for piezoelectric tube nanopositioners. *IEEE Transactions on Control Systems Technology*, 14 (1) (2006) 33 – 44.

P. E. Wellstead Introduction to Physical System Modelling. Academic Press, 1979.

S. O. R. Moheimani and S. Behrens Multimode piezoelectric shunt damping with a highly resonant impedance. *IEEE Transactions on Control Systems Technology*, 12 (3) (2004) 484–491.

C. A.Desoer, M. Vidyasagar Feedback Systems: Input-Output Properties. Academic Press, London, 1975.

P. J. Gawthrop and G. P. Bevan Bond-Graph Modeling: A tutorial introduction for control engineers, *IEEE Control Systems Magazine*, 27 (2) (2007), 24–45.